ASSESMENT OF SOURCE TERM AND TURBULENCE MODEL COMBINATIONS FOR FILM COOLING IN TURBINES

M. Müller - C. Morsbach

Institute of Propulsion Technology
German Aerospace Center (DLR)
Cologne, Germany

ABSTRACT

Modern gas turbines require an active cooling system with fluid taken from the compressor to withstand the high turbine inlet temperature. CFD is a useful tool to estimate the effects of different cooling configurations on the blade aerodynamics and the thermal loads. However, this usually requires resolving every cooling hole with a high number of grid cells. To reduce the computational cost of such simulations, a reduced order model using source terms was implemented in TRACE. Different variants are tested on a cylindrical and a laid back fan shaped cooling hole to address issues with accuracy and grid dependency known from the literature. Additionally, two different turbulence and heat flux model combinations are compared to each other. Overall, a differential Reynolds Stress Model with an algebraic heat flux model combined with the simplest approach to modeling film cooling holes, introducing a constant source term at the wall, provided the best results for the considered geometries and blowing ratios. The different strategies to improve the predictions were only able to provide a benefit for some of the cases, while usually having a detrimental effect in other cases.

KEYWORDS

CFD, FILM COOLING, TURBULENCE MODEL

NOMENCLATURE

CFD	Computational Fluid Dynamics	DR	Density Ratio
LES	Large Eddy Simulation	M	Blowing Ratio
RANS	Reynolds Averaged Navier Stokes	h	Enthalpy
RSM	Reynolds Stress Model	T	Temperature
URANS	unsteady RANS	η	Cooling Effectiveness

INTRODUCTION

Modern gas turbines require an active cooling system with fluid taken from the compressor to withstand the high turbine inlet temperature, above the melting point of the alloys used in the first rows of a high-pressure turbine. This fluid is not part of the full thermodynamic cycle and the turbine will extract less energy from it. Reducing the amount of coolant therefore increases efficiency. However, inadequate cooling can drastically reduce turbine life. Computational Fluid Dynamics (CFD) can help to optimize the amount and distribution of cooling fluid.

For an automated design optimization of cooled high pressure turbine blades, using a steady RANS approach is the only cost effective CFD method. However, RANS has known deficits

when predicting the complex interactions, both within and outside of a cooling hole. Jones et al. [1] summarized the literature with: "Typically they focus on the adiabatic effectiveness downstream of the hole which RANS is particularly bad at predicting, [...]". Unfortunately, the film cooling effectiveness is relevant for turbine designers. Comparing RANS to an implicit LES, Jones et al. [1] concluded that RANS is able to capture the velocity fields and predict the changes when the inflow angle is altered on a laid-back fan shaped hole. Nevertheless, RANS with the realizable k-ϵ model was unable to predict the mixing and spreading of the coolant. This may lead to problems estimating the thermal loads, e.g when assessing a cooled turbine blade.

The prediction of the cooling effectiveness in RANS simulations is strongly affected by the turbulence model. In addition, the heat flux model, which calculates turbulent heat transport based on turbulence model predictions, also has a large influence. Rouina et al. [2] compared several turbulence models on a laid-back fan shaped cooling hole to measurements and found that the Reynolds Stress model (RSM) available in Star-CCM+ outperformed all considered two equation eddy viscosity models. From a theoretical perspective, RSMs should have an advantage over common two equation eddy viscosity models. Instead of relying on the Boussinesq assumption that the Reynolds stresses follow the strain rate tensor scaled by the eddy viscosity, all six Reynolds stresses are treated individually. This allows for a better prediction in complex flows with high anisotropy such as separations, vortices or other 3D structures [3], which usually will be present in and around a coolant jet. Additionally, the Reynolds stresses are a necessary input for more complex heat flux models, e.g. those using the generalized gradient diffusion approach. Ling et al. [4] compared different heat flux models using an LES of a cylindrical cooling hole. They calculated the turbulent Prandtl number on the LES solution and found that it varied considerably from 0.2 to 1.5. They concluded that this undermined the application of the Reynolds analogy, meaning that the most common approach to modelling turbulent heat flux, using a constant turbulent Prandtl number, leads to large errors. When run on the velocity field, temperatures and Reynolds stresses extracted from the LES, other models using variations of the generalised gradient diffusion approach performed better. However, accuracy was still found to be lacking. In addition, the model by Daly and Harlow [5] failed to converge in a RANS simulation, with the authors questioning whether the extra effort required to implement and converge the more complex models was worth the gains in accuracy. In contrast, Brakmann et al. [6] found that the explicit algebraic RSM by Hellsten combined with that heat flux model performed better than Menter's SST k-ω model [7].

A steady-state RANS simulation of a cooled turbine requires a fraction of the computational power of, for example, an LES. However, it is unable to resolve the complex flow physics present in this application. Nevertheless, the computational cost of steady RANS with fine meshes resolving the cooling holes is still high when a large number of different simulations are required. For example, Lee et al. [8] optimised the cooling configuration on the pressure side of a nozzle guide vane. Computational cost was an issue in this study, the original 25 million cell grid had to be simplified by omitting the shower head, which removed just over half of the cooling holes in this stator design. Additionally, this particular design was for a comparatively small engine with around 45 kN thrust. Other designs are physically larger and require a different cooling layout, resulting in many times the number of cooling holes and grid cells. Thus, several authors have proposed reduced-order models to inject cooling fluid without resolving the individual cooling holes. This also allows for the use of the same grid to simulate multiple configurations of cooling holes, saving additional time and resources. However,

as reduced-order models, they trade some accuracy for the greater benefit of reduced computational cost. As such, they should be considered as one tool in a larger toolbox of CFD methods to be used when appropriate, where a more detailed approach is not feasible or cost effective. They could be particularly valuable as a low-fidelity method in a multi-fidelity optimisation. For example, in a Co-Kriging method as used by Schnös et al. [9], many CFD solutions using this model could be combined with few resolved simulations. This can reduce costs while still taking advantage of the better accuracy of the high fidelity methods.

Auf dem Kampe and Völker [10] proposed a complex but capable model for cylindrical cooling holes, based on adding a source term in a volume around the cooling hole exit. Both this volume and the source terms are defined by a correlation based on nine parameters describing the cooling hole and the flow conditions. The agreement between the model and resolved cooling hole was excellent on the considered test cases, however the actual parameters were not published. The approach itself, using either volume or surface sources to model a cooling jet, was used by different authors in simpler form. Andrei et al. [11] investigated a simplified version in two variants, one setting sources only in wall adjacent cells, the other in a volume around the cooling hole exit. They found the surface sources to be superior in both accuracy and grid dependency. Bizzari et al. [12] used a similar surface model to simulate effusion cooling in a combustion chamber LES. To deal with under-resolved cooling holes, they propose artificially increasing the hole diameter to better resolve the interaction of the jet and the crossflow.

As the available computing power continues to increase, the efficiency gained from such models can be reinvested in a more accurate solution of other flow physics. For example, Schmidt and Starke [13] showed the shortcomings of a steady-state RANS in predicting how heat is transported in a rotor-stator configuration subjected to a hot streak. However, the computational cost of time domain URANS simulations will continue to limit their use. A combination of non-linear frequency domain methods with a film cooling model could provide the necessary efficiency to incorporate them into, for example, a multi-fidelity optimisation. However, in the author's experience, frequency domain methods especially benefit from the use of robust and stable models. Therefore, the film cooling model presented in this paper is designed to be as simple and robust as possible. Nonetheless, it is combined with much more complex turbulence and heat flux models as these are reported to provide a significant increase in accuracy. Their applicability to frequency domain methods is a relevant question. However, this paper first attempts to evaluate their benefits when combined with a film cooling model.

Therefore, a simple approach comparable to Andrei et al. [11] is combined with a differential RSM and an algebraic heat flux model. The combination is applied to a cylindrical and a laid-back fan shaped cooling hole, both with several operating points. To investigate the observed differences between modelled and resolved cooling holes, the flow features neglected by the cooling model and the discrepancies in the vortex systems are discussed in more detail.

Methods

Two variants of a source term model have been implemented in DLRs turbomachinery CFD solver TRACE [14]. TRACE uses the finite volume approach to solve the Reynolds-averaged Navier-Stokes (RANS) equations. The density based, compressible solver attains second order accuracy using Roe's upwind scheme and a MUSCL extrapolation. A van Albada type flux limiter is used to smooth large gradients, e.g. in the vicinity of shocks. Two different combinations of turbulence and heat flux models are used. Menter's SST k-ω [7] model combined with a constant turbulent Prandtl number of 0.9 serves as a baseline. Compared to this is the seven

equation differential Reynolds Stress model SSG/LRR-ω proposed by Eisfeld et al. [3] combined with the algebraic heat flux model by Daly and Harlow [5]. For the solution of turbulence equations, a conservative, segregated method is used [15].

The implemented film cooling model is a simplification of the model proposed by auf dem Kampe [10] and similar to the one used by Andrei et al. [11]. Unlike the former, the sources of mass, momentum and energy for a given cooling hole are constant and homogeneous in the participating cells. Compared to the latter, the pressure at the exit of the coolant hole is not a user input. Instead, the user specifies the coolant mass flow $\dot{m}$, the coolant total temperature $T_{t,c}$, the direction of the cooling hole and its diameter or outlet area. From this input, the exit velocity u is calculated with the static pressure above the centre of the hole, assuming an isentropic expansion. The resulting equations for the source terms are identical to those presented by Becker et al. [16], with the improvement that the exit velocity and the region where the source terms are applied are determined by the model rather than being explicitly prescribed. This makes it possible to use the sources in a much more targeted manner, while still maintaining a high level of automation. The quantities are distributed volume weighted among all cells assigned to a particular coolinghole, with V_{model} being the total volume of all cells participating in the model. For a cell with index j, the source term $\hat{S}_j$

$$S_{\dot{m},j} = \frac{\dot{m}}{V_{\text{total}}} \cdot V_{\text{j}} \tag{1}$$

$$\hat{S}_{M,j} = S_{\dot{m},j}\hat{u} \tag{2}$$

$$S_{E,j} = S_{\dot{m},j}\left(h_{\text{coolant}} + \frac{1}{2}|\hat{u}|^2\right) \tag{3}$$

is introduced to the Navier Stokes equations

$$\frac{\partial}{\partial t}\int_V \hat{Q}dV + \int_S \hat{F}dS = \int_V \hat{S}dV \tag{4}$$

$$\hat{S} = [S_{\dot{m}}, \hat{S}_{M,i}, S_E] \tag{5}$$

with $\hat{Q}$ the vector of conservative variables and $\hat{F}$ the vector of Euler and viscous fluxes.

To complete the model, a region has to be defined where this source term is applied. Two different approaches were implemented, one setting sources only directly adjacent to the surface and one extending this region into a volume above the cooling hole exit. The sum of mass, momentum and energy is exactly the same between the two variants implemented here, but the effect of the model is more spread out with the volume source variant. There may be two potential advantages to such an approach. First, with a less localised source term, gradients between cells that participate in the model and adjacent ones will be reduced. This could lead to better robustness and a more accurate solution. Secondly, as discussed in the introduction, insufficient mixing is one of the problems in correctly predicting film cooling flows with RANS in general and with a cooling model in particular. Expanding the volume can artificially provide some of the mixing missing from these simulations. However, similar to what Andrei et al. found, this approach did not reliably provide an advantage. As this has already been addressed in the literature, this variant will not be discussed in detail in this paper. The surface variant used in the following sections may also be more desirable from a modelling point of view, as it is completely free of parameters that need to be fitted. This also means that no model parameters can be inadvertently used in flow conditions for which they have not been calibrated.

A source term is added to individual cells under two conditions. First, the cell must be adjacent to the wall with the cooling hole. Second, the centre of the cell must be above the exit of the cooling hole. Additionally, a slip wall condition is applied where the model is active. This is set individually for each cell and the boundary condition is only applied to cells that are involved in the model. A no-slip condition would be in competition with the source terms set by the film cooling model and would lead to a false influx of momentum into the domain. This results in a minimal computational cost for the model. The cells and source terms can be determined once at the start of the simulation. After that, adding the sources in a small number of cells causes negligible overhead. Thus, the cost reduction achieved by using the model is directly proportional to the reduction in mesh cells.

To address some of the issues discussed in the results section, the artificial increase of the cooling hole diameter to ensure a minimum grid resolution proposed by Bizzari et al. [12] was implemented and tested. The number of cells across the lateral direction of the cooling hole is counted. If a set minimum resolution is not reached, the diameter is iteratively increased until enough cells will participate in the model.

The capabilities and limitations of the cooling models will be discussed primarily based on the laterally averaged film cooling effectiveness $\bar{\eta}$. This quantity is obtained by averaging the film cooling effectiveness at the wall for each x/D.

$$\eta = \frac{T_\infty - T_{aw}}{T_\infty - T_c} \tag{6}$$

where T_{aw} denotes the temperature at the adiabatic wall and T_c that of the coolant.

Test Cases

Two different geometries are considered for this paper. Firstly, the cylindrical film cooling hole investigated by Baldauf et al. [17] is simulated as a resolved cooling hole including a plenum and with the source term models. The case with an angle of 30° and a hole spacing $s/D = 3$ was chosen. Several grid resolutions are investigated for both variants, since a substantial grid dependency is a known issue when using surface or volume sources to model film cooling holes. Additionally, the geometry investigated by Schroeder and Thole [18] is used here to test the methods on a laid back fan shaped cooling hole. Not all of the different operating points investigated experimentally are considered in this paper. The operating points simulated here are summarized into Tab. 1 for both geometries.

The geometry of the cylindrical cooling hole considered by Baldauf et al. is shown in Figure 1a and the 777 laid-back fan-shaped cooling hole considered by Schroeder and Thole is shown in Figure 1b. In both cases the coolant is injected from the bottom of the plenum by a homogeneous boundary condition. The inlet to the hot gas duct is also homogeneous, a boundary layer profile is developed over an inlet surface length chosen to approximate the boundary layer thicknesses measured in the experiment. Importantly, $x/D = 0$ is defined as the centre of the cooling hole exit in the Baldauf case, but as the trailing edge of the cooling hole in the Schroeder and Thole case. This was retained for the simulations.

Structured multi-block grids are used for all cases considered. The resolved cooling holes are meshed with an O-H grid, which is extended into the hot gas channel and the plenum. Those grids will be references as "Resolved". For the modelled cooling holes, the grids are uniform in the lateral direction and sufficiently fine to resolve the boundary layer with a low-Re boundary condition. These grids are refined by increasing the number of cells in the stream-wise and

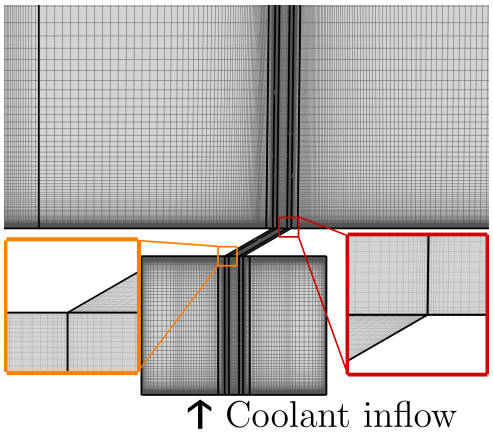

(a) Cylindrical cooling hole

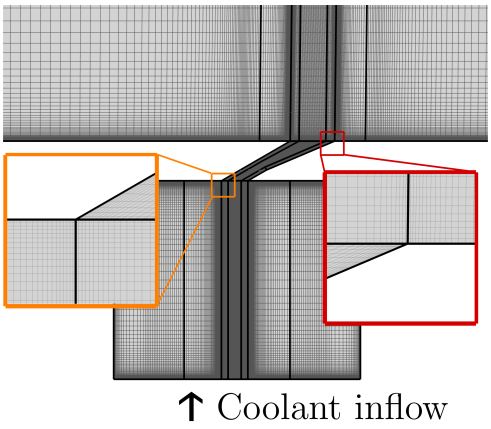

(b) 777 laid-back fan shaped cooling hole

Figure 1: Computational domain and grids around the injection region. Block borders are marked with black lines.

in the lateral direction. The wall normal direction, and therefore y^+, is left constant. Those grids will be referenced as "Model Grid". For resolved cooling holes, the refinement is done in three dimensions leaving y^+ constant. Tab. 2 presents the grid parameters. Grids for modelled cooling holes will be identified by the number of cells available to resolve a cylindrical film cooling hole in the lateral direction. The resolved grids have a boundary layer refinement in the cooling hole, so the cell count in the lateral direction is no longer a very intuitive measure of grid resolution. Instead, the grids will be identified by their relative cell count.

Table 1: Flow Conditions

Variable	Baldauf	Schroeder
Blowing ratio (M)	0.5, 1	0.5, 1, 2
Density ratio (DR)	1.5	1.5
Mainstream velocity	60 m/s	10 m/s
Turbulence Intensity	1.5%	5.4%

Table 2: Grids

Name	Cell count	y^+
Resolved 1	2,700,00	≈ 0.9
Resolved 2	5,200,000	≈ 0.9
Resolved 4	10,800,000	≈ 0.9
Model Grid 1	60,000	≈ 0.4
Model Grid 3	260,000	≈ 0.4
Model Grid 5	600,000	≈ 0.4
Model Grid 7	1,090,000	≈ 0.4
Model Grid 15	4,500,000	≈ 0.4
Model Grid 23	10,150,000	≈ 0.4

Results

The differences between the two turbulence and heat flux model combinations are best visible in the lateral spread of the cooling film. Fig. 2 depicts the cooling efficiency for both models on the finest grid of the resolved cylindrical cooling hole in a distorted view. Both turbulence models predict a separation of the cooling film, with the maximum η further downstream from the hole exit. However, the Reynolds Stress model reaches this point at a lower x/D, agreeing better with the experimental data of Baldauf [17]. Another visible advantage of the Reynolds stress model is the improved lateral spread of the coolant, which also leads to a lower centerline film cooling efficiency downstream of $x/D \approx 30$. This indicates that the model combination is indeed able to better predict the mixing and diffusion in a cooling film.

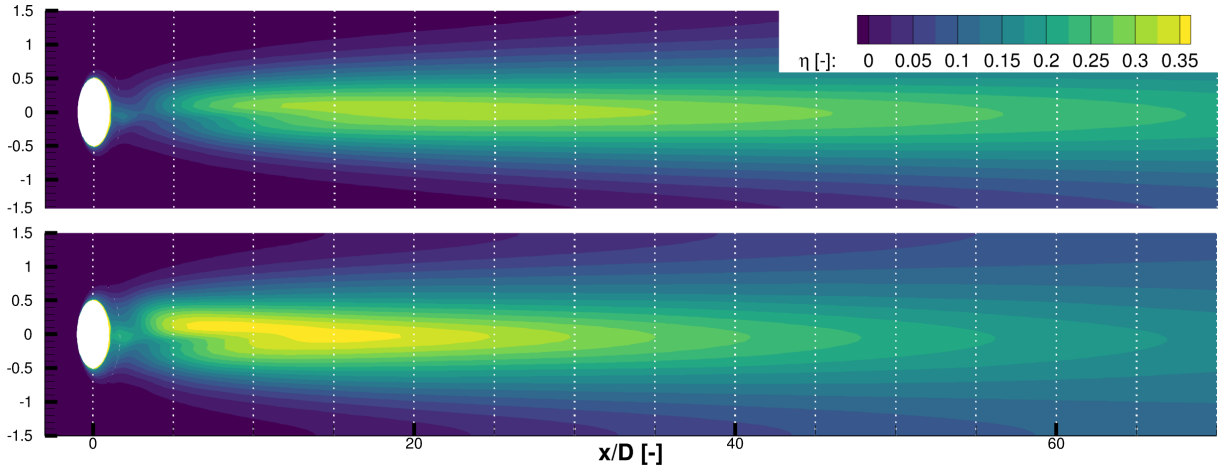

Figure 2: Film cooling effectiveness for SST (top) and SSG/LRR-ω with the Daly-Harlow heat flux model

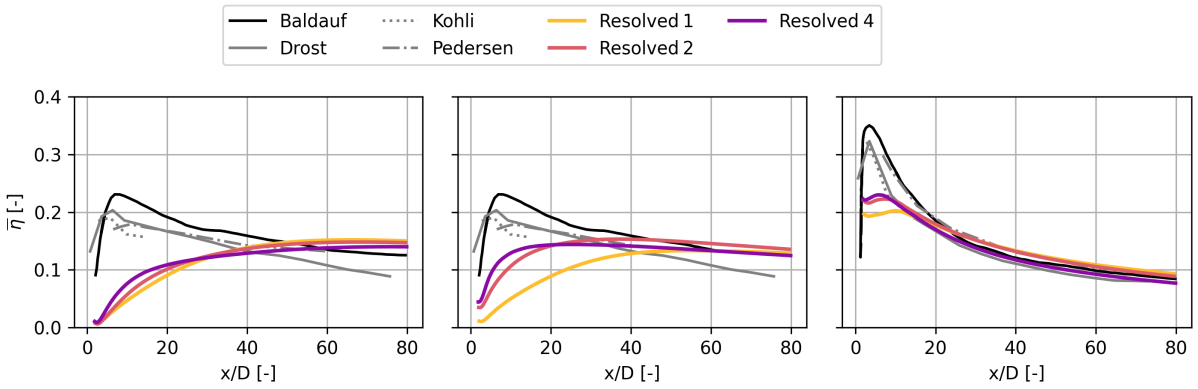

(a) M 1 SST (b) M 1 SSG/LRR+DH (c) M 0.5 SSG/LRR+DH

Figure 3: Laterally averaged film cooling effectiveness for the resolved cylindrical cooling hole

The asymmetry present in both simulations is unexpected for a steady RANS on a symmetric problem. A URANS simulation was carried out to ensure that steady RANS was suitable for solving this problem. It developed a very similar asymmetric but steady solution. This is not unique to this paper, a similar asymmetry can also be seen in some of the literature. E.g. in Ling et al.[4] for both steady RANS and LES. This indicates that slight asymmetries in the grid or numerical fluctuations could cause the flow to attach to any side of the cooling hole.

The laterally averaged film cooling efficiency for several grid resolutions is shown in Fig. 3a and 3b. Experimental data for several similar geometries, blowing ratios and density ratios is depicted in addition to the data from Baldauf et al. [17]. The data for the measurements of Drost et al., Kohli et al. and Pedersen et al. is reproduced from the publication of Baldauf. Those experiments are not completely identical to those of Baldauf et al. [17]. Differences are, for example, the approaching boundary layer or a density ratio of 1.6. Nonetheless, the differences between the measurements with DR=1.6 are greater than the respective differences to Pedersen's measurement at DR=1.5. This range of experimental results can serve as a guideline to determine what deviations between the different simulation methods are acceptable.

Considering the experimental data plotted in black and grey in Fig. 3a, a good qualitative

agreement between the different measurements can be observed. However, the absolute values are different. In all experiments, the cooling jet detaches from the wall, but quickly reattaches close to the cooling hole. In the case of the Baldauf data, this is around the maximum value of the laterally averaged film cooling effectiveness at $x/D \approx 7$. Downstream of this point the cooling film mixes out, reducing the film cooling effectiveness. The resolved simulations in Fig. 3a predict a different behaviour of the cooling film. With the SST turbulence model, there is no definitive reattachment point. The maximum film cooling effectiveness visible in Fig. 2 may seem to indicate a reattachment region. However, the core of the jet sits above the surface and cool fluid is mixed into the boundary layer. This results in a slow increase of the cooling effectiveness without a well defined peak. The combination of the SSG/LRR-ω model with the heat flux model in Fig. 3b performs better, but still shows the same deficits. Close to the cooling hole the effectiveness is predicted better than with the SST model, the error is reduced by around a third. However, this is still a substantial under-prediction. For $x/D \approx> 35$, the prediction lies in the range of experimental results. Even so, the physics of the problem are not correctly captured and the slope of the RANS prediction does not match the experimental results. The cooling jet never reattaches, it is still a detached jet that mixes down towards the surface. For comparison, with a reduced blowing ratio in Fig. 3c, the simulations can capture the behaviour of the cooling jet much better. They agree with the experimental data closer to the cooling hole and, with the RSM and heat flux model, also capture the slope further downstream.

Fig. 3a-3c illustrate some of the known deficits of RANS when simulating these kinds of flows. Especially the detachment and reattachment of the cooling jet is difficult to predict [1][19]. For a low blowing ratio, this is less of a problem. The cooling film will stay attached under most circumstances and this stable behaviour leads to smaller errors. Conversely a high blowing ratio, e.g. 3 as considered by Mazzei et al. [19], reportedly leads to a reliably detached jet, which RANS simulations can again capture. It is in between these clear cases that the deficits are most visible. This results in the errors in the averaged film cooling effectiveness for a blowing ratio of 1, where the behaviour of the cooling jet is mispredicted. It is therefore useful to consider the total error between simulation and experiment as being composed of two parts. On the one hand, the behaviour of the cooling film directly at the injection point, i.e. a possible detachment and reattachment and the initial mixing, would have to be reproduced correctly. On the other hand, the transport and diffusion, further downstream of the injection point, also has to be reproduced correctly. From the simulations of the resolved cooling holes we can conclude that the RSM combined with the heat flux model offers some advantages in the first part, the initial mixing process, and more substantial improvements in predicting the mixing further downstream. For the test cases considered in this paper, it can deliver its theoretical advantages. Therefore, the film cooling model will be used with the RSM and heat flux model in the following sections. The resolved cooling holes in Fig. 3a-3c can also serve as a better reference for the source term models in the following sections.

Neglected flow phenomena

Running the model on the resolved grid can provide some insight as to what differences are to be expected and why they develop. Plenum and cooling hole are removed from the domain and replaced by a source term. The cell refinement around the exit is kept and the interaction of the cooling jet with the hot fluid can be resolved. However, the inner structure of the cooling jet is now completely missing. The results are plotted in Fig. 4. For both blowing ratios, the solution on this grid is very similar to that of the finest grids used with the model.

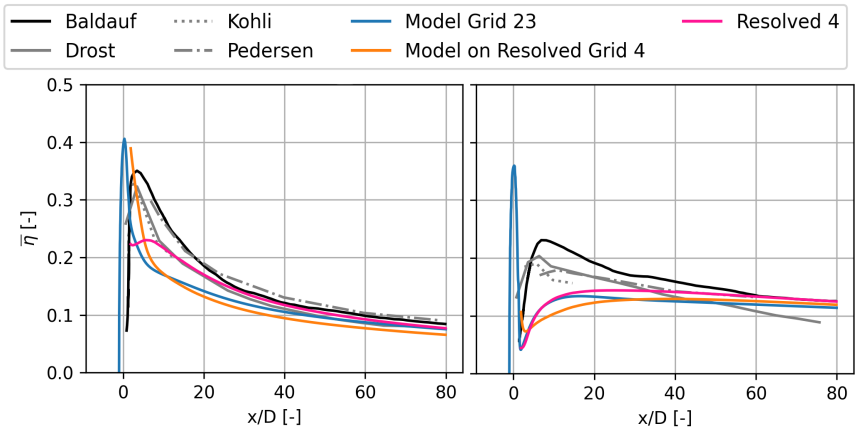

(a) M 0.5 SSG/LRR+DH (b) M 1 SSG/LRR+DH

Figure 4: Averaged film cooling effectiveness for the modelled cylindrical cooling hole

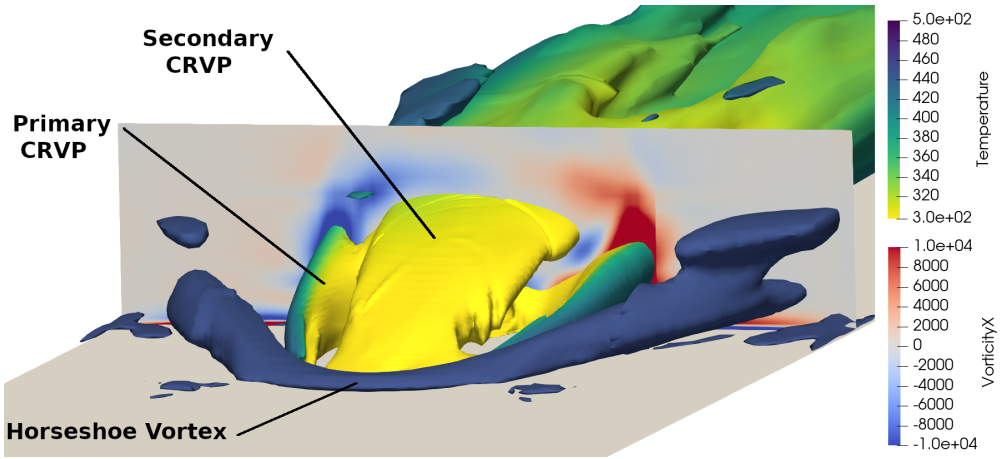

Figure 5: Vortex structures at the cooling hole exit for a resolved cylindrical cooling hole with a blowing ratio of 1 with SSG/LRR-ω and Daly-Harlow heat flux model

The difference between modelled and resolved cooling holes are primary the result of two related mechanisms, that are neglected in the simple source term models considered here. The general flow phenomena are the same for both geometries, however their exact expression and strength differs between the two geometries. The vortex structures of the cylindrical cooling hole at a blowing ratio of 1 are visualized in Fig. 5. The first neglected phenomena is the counter rotating vortex pair (CRVP) already present when the cooling jet exits the hole. This vortex originates at the inlet to the cooling hole and is marked as secondary CRVP in Fig. 5. Additionally, the horseshoe vortex at the start of the cooling hole is visible. The primary CRVP is partially obscured by the vortex pair exiting the cooling hole. This primary vortex transports hot fluid towards the surface and under the cooling jet. Furthermore, it also transports fluid upwards at the centerline, therefore strongly influencing if and how the coolant jet detaches from the wall. The CRVP is stronger at higher blowing ratios which reduces the cooling efficiency.

The interaction of the two CRVPs is visible in the vorticity field depicted in Fig. 6a. The secondary CRVP in the center is also rotating in the opposite direction compared to the primary CRVP. This secondary CRVP tries to push the jet core down towards the wall. Even though it

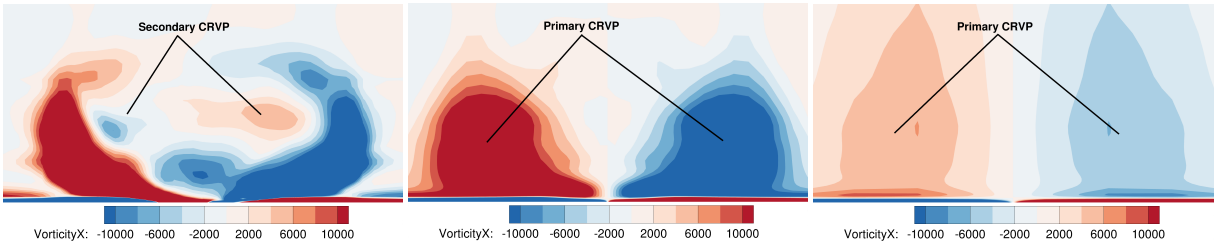

(a) Resolved (b) Model grid 15 (c) Model grid 3

Figure 6: Vorticity field at the trailing edge of the cylindrical cooling hole ($x/D = 0.5$) with SSG/LRR-ω and Daly-Harlow

is overcome by the primary vortex pair, it still affects the film cooling efficiency. Due to the homogeneous sources used in the cooling model, the secondary CRVP is missing in Fig. 6b. This grid is still sufficient to resolve the primary CRVP when the cooling model is used, although its position as shifted closer to the centerline. Without the interference from the secondary CRVP, the jet core is pushed upwards and hot fluid has better access to the surface beneath the jet. This results in the reduced film cooling efficiency of the model visible for $M = 1$. On coarser grids, as pictured in Fig. 6c for a grid resolution of 3 cells per diameter, the primary CRVP can not be properly resolved and is weakened. This results in an over-prediction of the cooling efficiency compared to the finer grids. This process is less relevant at low blowing ratios, since the secondary CRVP is weaker. Consequently, a lower grid dependency and a closer match of resolved and modelled film cooling hole can be observed for $M = 0.5$ on both geometries.

The second neglected effect is visible in Fig. 7 for the laid back fan shaped cooling hole. In the resolved cooling hole the distribution of the coolant is not homogeneous. This is closely related to the secondary CRVP, as the inner structure of the coolant jet also determines how most of the coolant is distributed. In the case of a blowing ratio of 0.5, the jet is comparatively weak and hot gas enters the cooling hole at the leading edge (Fig. 7a). Much of the flux out of the cooling hole is at the trailing edge. Compared to this, the flow physics is very different for a blowing ratio of 2 (Fig. 7b). There is no hot gas ingestion, instead most of the coolant exits near the leading edge at a much higher velocity. This change from low to high blowing ratio is caused by a constriction of the flow path by a vortex in the diffusor part of the cooling hole. As a result, the jet exits with a much higher velocity compared to a uniform distribution. As this occurs at the leading edge, it also affects the formation of the primary CRVP after the jet exits the cooling hole. This inhomogeneity is more pronounced at higher blowing ratios and moves towards the leading edge as the blowing ratio increases, contributing to the errors observed between resolved and modelled film cooling holes at high blowing ratio.

Modeling the cylindrical cooling hole

The laterally averaged film cooling efficiency obtained with the source term model is shown in Fig. 8a for $M = 0.5$ and in Fig. 8b for $M = 1$. As with the resolved cooling hole, the experimental data is better reproduced further downstream for both blowing ratios. Similar to the model on the resolved grid in Fig. 3b, the discrepancy between the model and the resolved cooling hole is significantly higher for $M = 1$. The sensitivity of the cooling film is also evident when using the cooling model at this blowing ratio. The different grid resolutions agree with the resolved film cooling hole on the overall physics of the cooling film. It always detaches without

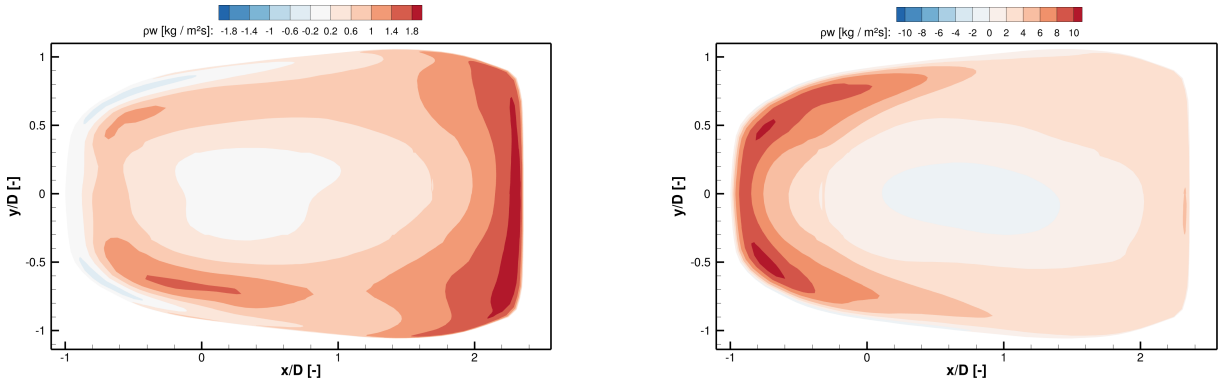

(a) M 0.5 (b) M 2

Figure 7: Momentum flux across the 777 cooling hole exit. Resolved cooling hole with SSG/LRR-ω and Daly-Harlow

a well defined reattachment point. However, the exact film cooling effectiveness depends on how far the core of the jet detaches and how well the different mixing processes are represented at the different grid resolutions, resulting in a shift of the different curves. This grid dependency is better visible in Fig. 9, where the cooling effectiveness is plotted over the grid resolution for several x/D. As reported in the literature, there is a significant grid dependency. The grid convergence behaviour is also oscillatory, converging towards the solution of the model on the resolved grid. Fig. 9 also demonstrates the effects discussed for Fig. 6c, low grid resolutions tend to overpredict the cooling efficiency, due to the inability to properly resolve the CRVP. Conversely, high grid resolutions tend to underpredict efficiency due to the missing secondary CRVP. Therefore, the model dies not converge against the result of the resolved cooling hole.

From a practical perspective, where the model may better be compared against the experimental data, the general deficits of RANS can also be observed in the model. Consequently, the model fails to predict the efficiency in vicinity of the cooling hole. The model may be considered trustworthy for $x/D \approx> 20$ at low M, where the errors are equivalent to the spread of the experimental data. For higher blowing ratios this point moves further downstream while the grid dependency increases. Additionally, the better performance of the SSG/LRR-ω model observed on the resolved cooling hole is repeated with the film cooling model.

Fig. 10 presents the results obtained with the thickened hole model adapted from Bizzari et al. [12]. Artificially increasing the hole diameter may allow for a better prediction of the mixing processes on very coarse grids. More cells may provide the ability to resolve the vortex system, at least to some degree. Additionally, from a purely practical point of view, distributing the sources over a larger area may help to better represent initial mixing for the $M = 1$ case. A distributed source term may lead to a cooling jet that is less prone to detach.

For very coarse meshes, thickening the cooling holes improves the prediction. Of course, increasing the size of the cooling hole also increases the laterally averaged film cooling effectiveness at the injection point. However, for a blowing ratio of 1, artificially increasing the hole diameter can have a detrimental effect. For a grid resolution of three cells per diameter, the cooling effectiveness was already overpredicted. This error is amplified when using the model. In addition, the behaviour the film cooling jet does not match the detachment and reattachment observed in experimental results and the reference RANS. The dependence on the grid itself becomes more marked as the curves move further apart.

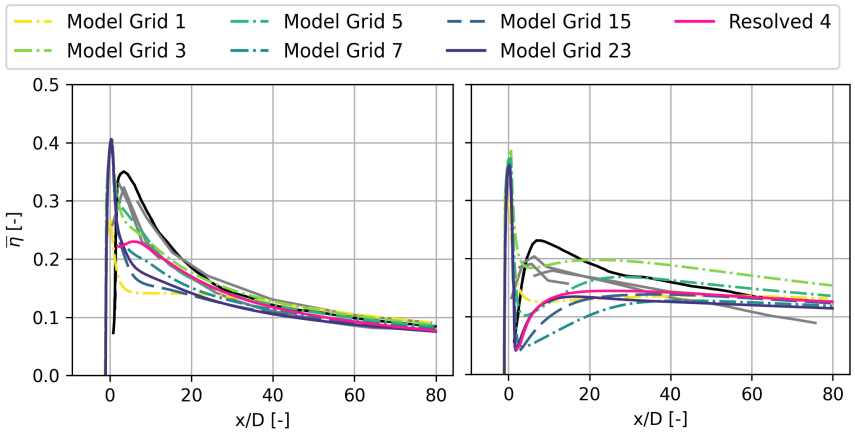

(a) M 0.5 SSG/LRR+DH (b) M 1 SSG/LRR+DH

Figure 8: Film cooling efficiency on the modelled cylindrical hole for different grid resolutions

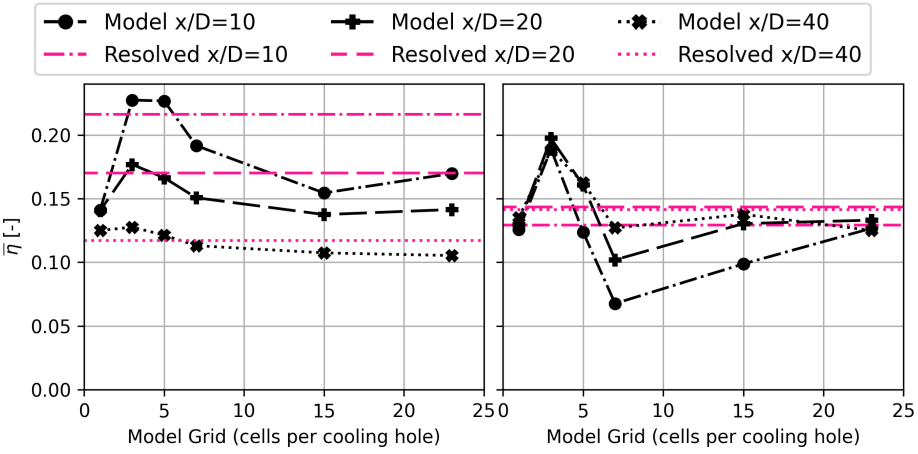

(a) M 0.5 SSG/LRR+DH (b) M 1 SSG/LRR+DH

Figure 9: Effect of grid refinement on the cooling efficiency at several x/D of the modelled cylindrical cooling hole

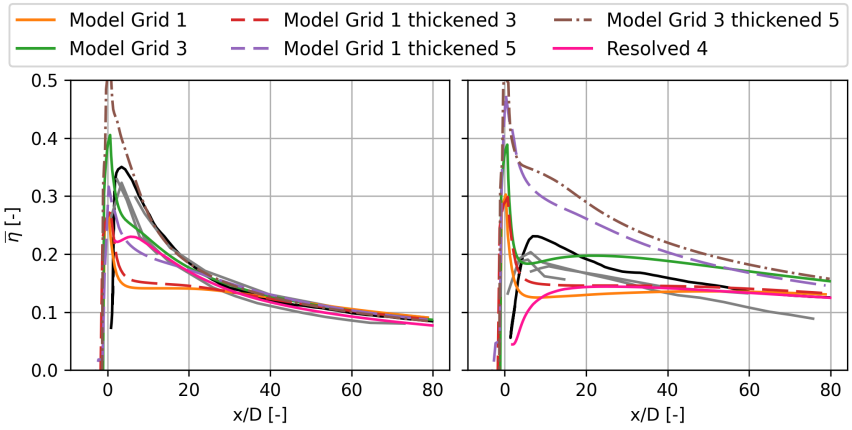

(a) M 0.5 (b) M 1

Figure 10: Effect of the thickened hole model on a cylindrical cooling hole at different grid resolutions

The thickened hole mode in this form is not a sure way to reduce the grid dependency, nor is it a reliable tool to approach the problems of RANS in predicting the behaviour of the coolant jet. However, for a grid resolution of only one cell, increasing the diameter to match 3 cells improved the results in all cases and combinations considered here. The basic physics of the coolant jet was not changed. Therefore, the detachment of the jet could still not be predicted. However, since this grid always underpredicted the film cooling efficiency, increasing the hole diameter brought the results closer to both the resolved hole and the experimental results. Bizzari et al. [12] also found a resolution of three cells per diameter to be a good minimum resolution, below which the cooling hole diameter is increased. That paper considered the very different problem of resolving effusion cooling in combustors with LES. Nevertheless, the same conclusion can be drawn from the cases considered here, indicating that artificially increasing the cooling hole diameter may be of practical value as insurance against severe under-resolution when grids become unintentionally coarse.

Modelling the laid back fan-shaped cooling hole

The results of the model and the resolved cooling hole are plotted in Fig. 11 for the three blowing ratios considered. In general, most of the trends mirror those observed for the cylindrical case. For the resolved cooling holes, a notable difference is the good agreement even close to the cooling hole exit. The physics of the film cooling jet seems to be correctly represented for the resolved cooling holes, although the $M = 2$ (Fig. 11c) case starts to deviate. Due to the stable behaviour of the cooling jet, RANS provides better results on this geometry. The jet is never fully detached for the blowing ratios considered. The model performs well for $M = 0.5$, where the internal structure of the cooling jet is weakest. As discussed earlier, this also reduces the grid dependency. Increasing the blow ratio leads to a stronger CRVP in the cooling hole and increases the inhomogeneity of the jet. This is not represented in the model. As with the cylindrical hole, this leads to a higher errors and a stronger grid dependency. Overall, the model remains usable at $M = 1$, but one has to be aware of the effects of insufficient grid resolution. This worsens at high M, with both severe under- and over-prediction of cooling efficiency.

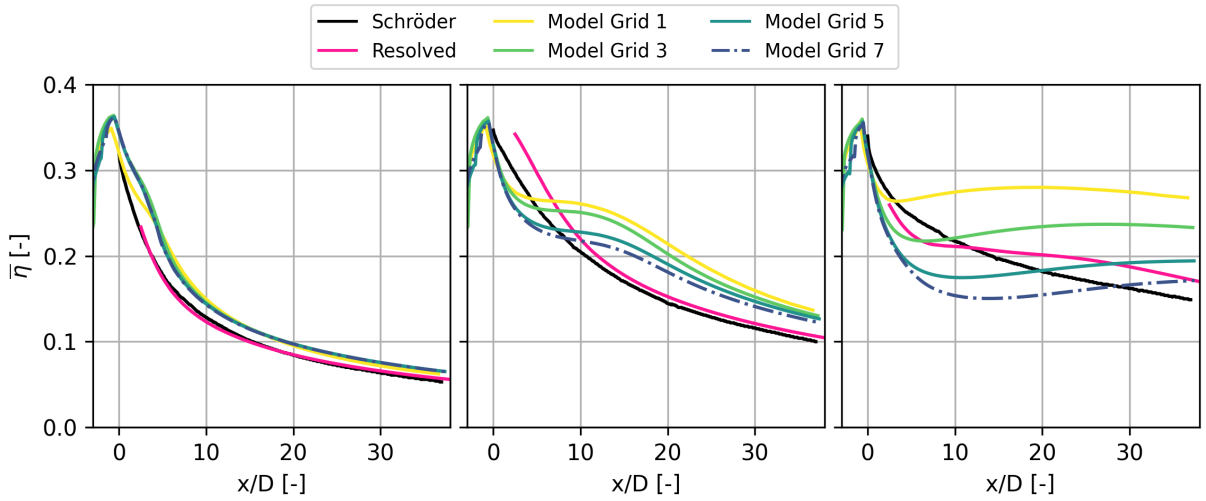

(a) M 0.5 SSG/LRR+DH (b) M 1 SSG/LRR+DH (c) M 2 SSG/LRR+DH

Figure 11: Laterally averaged film cooling effectiveness for the modelled 777 cooling hole

Conclusions

When evaluating the combination of models, it is useful to distinguish between two types of error: Firstly, how well the injection is reproduced and secondly, how good the downstream mixing is. The film cooling model is mainly responsible for the first part and works well at small blowing ratios. However, the assumptions made for the model, i.e. a homogeneous cooling jet with uniform direction, do not hold for high blowing ratios. Under those conditions the film cooling model cannot be considered trustworthy close to the injection point. Only from $x/D = 20$ onwards does the model approximate the results of the resolved cooling hole. With three to five cells to resolve the cooling hole, a good approximation to the measurement results can be observed due to the mutual elimination of several errors, even at a high blowing ratio. However, this is accompanied by large uncertainties on meshes with less than 7 cells per cooling hole, especially at a blowing ratio of 2. However, much finer meshes for the model have a similar number of cells as the resolved cooling hole, which makes the use of the model less attractive. But without a model any change in geometry requires a new mesh to be created. Artificially increasing the diameter of the cooling hole according to the approach of Bizzari et al. did not reliably improve results. However, this approach may still be of practical value for film cooling holes, as a fall-back to limit errors caused by unintentionally coarse meshes.

Secondly, the mixing downstream of the cooling hole, is significantly improved by combining SSG/LRR-ω with the Daly and Harlow heat flux model compared to Menter's SST k-ω model with a constant turbulent Prandtl number, whether the cooling hole is modelled or resolved. If the computational resources to run a differential Reynolds Stress model are available, the use of such a combination can be recommended on the basis of the present results. The lack of robustness of the RSMs reported in the literature could not be observed here.

The identified deficiencies in the representation of vortex structures could be used to further improve the model. However, a deliberate choice was made to keep the model as simple and robust as possible. Since the CRVP was significantly weakened on the coarsest meshes, it seems likely that introducing the vortices through a source term would require fine meshes. This would lead to the exclusion of some of the coarser meshes from this study, where a simplified approach

still provides useful results at lower blowing ratios. In terms of robustness, the model met its stated objectives as no problems were observed.

To evaluate the usefulness of the film cooling model, both the limitations of the model and the available alternatives should be considered. For the outlined use as part of a multi-fidelity optimisation, the model is not in direct competition with a well-resolved RANS or more expensive methods. Instead, other reduced-order approaches such as modelling via correlations or via large-scale homogeneous source terms are more comparable. The model can represent the effect of a cooling hole much more locally and partially resolve the relevant flow phenomena. To help make a decision on this, further investigations on cooled blades are planned.

ACKNOWLEDGEMENTS

The authors would like to thank Robert P. Schroeder for access to the experimental data on the 777 cooling hole.

REFERENCES

References

[1] F. B. Jones, D. W. Fox, and D. G. Bogard, "Evaluating the Usefulness of RANS in Film Cooling," vol. Volume 5A: Heat Transfer of *Turbo Expo: Power for Land, Sea, and Air*, 06 2019. V05AT12A019.

[2] S. Rouina, S. Ravelli, and G. Barigozzi, "Combined experimental and cfd investigation of flat plate film cooling through fan shaped holes," *International Journal of Turbomachinery, Propulsion and Power*, vol. 4, no. 2, 2019.

[3] B. Eisfeld, "The influence of the length scale equation on the simulation results of aerodynamic flows using differential reynolds stress models," in *New Results in Numerical and Experimental Fluid Mechanics VII* (A. Dillmann, G. Heller, M. Klaas, H.-P. Kreplin, W. Nitsche, and W. Schröder, eds.), (Berlin, Heidelberg), pp. 83–90, Springer Berlin Heidelberg, 2010.

[4] J. Ling, K. J. Ryan, J. Bodart, and J. K. Eaton, "Analysis of turbulent scalar flux models for a discrete hole film cooling flow," *Journal of Turbomachinery*, vol. 138, oct 2015.

[5] B. J. Daly and F. H. Harlow, "Transport equations in turbulence," *Phys. Fluids*, vol. 13, no. 11, pp. 2634–2649, 1970.

[6] R. G. Brakmann, R. Schöffler, F. Kocian, M. Schroll, C. Willert, M. Müller, and E. Kügeler, "Quantitative Flow Imaging of Film Cooling Jets in a Cross-Flow Using Particle Image Velocimetry and Computational Fluid Dynamics," vol. Volume 7B: Heat Transfer of *Turbo Expo: Power for Land, Sea, and Air*, 09 2020. V07BT12A069.

[7] F. R. Menter, "Two-equation eddy-viscosity turbulence models for engineering applications," *AIAA J.*, vol. 32, pp. 1598–1605, Aug. 1994.

[8] S. Lee, D.-H. Rhee, B. J. Cha, and K. Yee, "Film cooling performance improvement with optimized hole arrangement on pressure side surface of nozzle guide vane: Part i — optimization and numerical investigation," in *Volume 5C: Heat Transfer*, American Society of Mechanical Engineers, jun 2016.

[9] M. Schnoes, A. Schmitz, G. Goinis, C. Voß, and E. Nicke, "Strategies for multi-fidelity optimization of multi-stage compressors with throughflow and 3d cfd," in *ISABE 2019*, September 2019.

[10] T. a. d. Kampe and S. Völker, "A Model for Cylindrical Hole Film Cooling—Part II: Model Formulation, Implementation and Results," *Journal of Turbomachinery*, vol. 134, 09 2012. 061011.

[11] L. Andrei, L. Innocenti, A. Andreini, B. Facchini, and L. Winchler, "Film Cooling Modeling for Gas Turbine Nozzles and Blades: Validation and Application," *Journal of Turbomachinery*, vol. 139, 09 2016. 011004.

[12] R. Bizzari, D. Lahbib, A. Dauptain, F. Duchaine, L. Y. M. Gicquel, and F. Nicoud, "A thickened-hole model for large eddy simulations over multiperforated liners," *Flow, Turbulence and Combustion*, vol. 101, no. 3, pp. 705–717, 2018.

[13] M. Schmidt and C. Starke, "Comparison of Steady and Unsteady Coupled Heat-Transfer Simulations of a High-Pressure Turbine Blade," vol. Volume 5A: Heat Transfer of *Turbo Expo: Power for Land, Sea, and Air*, June 2015. V05AT10A016.

[14] K. Becker, K. Heitkamp, and E. Kügeler, "Recent Progress In A Hybrid-Grid CFD Solver For Turbomachinery Flows," in *Proceedings Fifth European Conference on Computational Fluid Dynamics ECCOMAS CFD 2010*, (Lisbon, Portugal), June 2010.

[15] C. Morsbach and F. di Mare, "Conservative segregated solution method for turbulence model equations in compressible flows," in *6th European Congress on Computational Methods in Applied Sciences and Engineering (ECCOMAS 2012)*, (Vienna, Austria), Sept. 2012.

[16] K. Becker, G. Ashcroft, S. Rochhausen, A. Weber, J. Rodriguez, and G. Schmid, "On the Application of a Harmonic Balance Method with a Volume Source Cooling Model to the Simulation of a Film-Cooled Turbine Stage," in *Proceedings of ASME Turbo Expo 2016*, no. GT2016-57199, (Seoul, South Korea), ASME, June 2016.

[17] S. Baldauf, A. Schulz, and S. Wittig, "High-Resolution Measurements of Local Effectiveness From Discrete Hole Film Cooling ," *Journal of Turbomachinery*, vol. 123, pp. 758–765, 02 1999.

[18] R. P. Schroeder and K. A. Thole, "Adiabatic Effectiveness Measurements for a Baseline Shaped Film Cooling Hole," *Journal of Turbomachinery*, vol. 144, 09 2022. 121003.

[19] L. Mazzei, A. Andreini, and B. Facchini, "Assessment of modelling strategies for film cooling," *International Journal of Numerical Methods for Heat & Fluid Flow*, vol. 27, pp. 1118–1127, Jan. 2017.